

pubs.acs.org/ac Article

MATRESHCA: Microtesla Apparatus for Transfer of Resonance Enhancement of Spin Hyperpolarization via Chemical Exchange and Addition

Shiraz Nantogma,* Md Raduanul H. Chowdhury, Mohammad S. H. Kabir, Isaiah Adelabu, Sameer M. Joshi, Anna Samoilenko, Henri de Maissin, Andreas B. Schmidt, Panayiotis Nikolaou, Yuri A. Chekmenev, Oleg G. Salnikov, Nikita V. Chukanov, Igor V. Koptyug, Boyd M. Goodson, and Eduard Y. Chekmenev*



Cite This: Anal. Chem. 2024, 96, 4171-4179



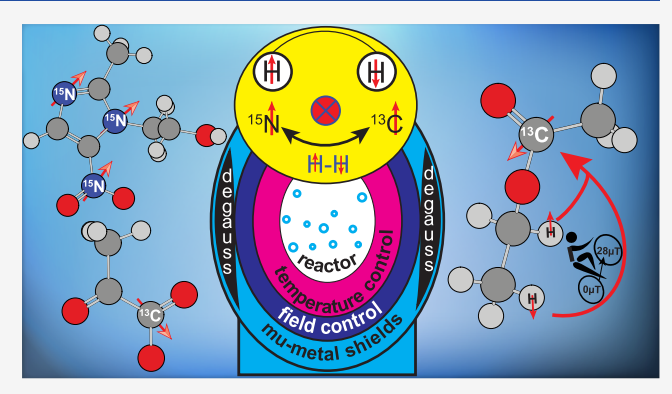
ACCESS

Metrics & More

Article Recommendations

s Supporting Information

ABSTRACT: We present an integrated, open-source device for parahydrogen-based hyperpolarization processes in the microtesla field regime with a cost of components of less than \$7000. The device is designed to produce a batch of ¹³C and ¹⁵N hyperpolarized (HP) compounds via hydrogenative or non-hydrogenative parahydrogen-induced polarization methods that employ microtesla magnetic fields for efficient polarization transfer of parahydrogen-derived spin order to X-nuclei (e.g., ¹³C and ¹⁵N). The apparatus employs a layered structure (reminiscent of a Russian doll "Matryoshka") that includes a nonmagnetic variable-temperature sample chamber, a microtesla magnetic field coil (operating in the range of 0.02–75 microtesla), a three-layered mumetal shield (to attenuate the ambient magnetic field), and a



magnetic shield degaussing coil placed in the overall device enclosure. The gas-handling manifold allows for parahydrogen-gas flow and pressure control (up to 9.2 bar of total parahydrogen pressure). The sample temperature can be varied either using a water bath or a PID-controlled heat exchanger in the range from -12 to 80 °C. This benchtop device measures 62 cm (length) × 47 cm (width) × 47 cm (height), weighs 30 kg, and requires only connections to a high-pressure parahydrogen gas supply and a single 110/220 VAC power source. The utility of the device has been demonstrated using an example of parahydrogen pairwise addition to form HP ethyl $[1^{-13}C]$ acetate $(P_{13C} = 7\%, [c] = 1 \text{ M})$. Moreover, the Signal Amplification By Reversible Exchange in SHield Enables Alignment Transfer to Heteronuclei (SABRE-SHEATH) technique was employed to demonstrate efficient hyperpolarization of ^{13}C and ^{15}N spins in a wide range of biologically relevant molecules, including $[1^{-13}C]$ pyruvate $(P_{13C} = 14\%, [c] = 27 \text{ mM}), [1^{-13}C] - \alpha$ -ketoglutarate $(P_{13C} = 17\%), [1^{-13}C]$ ketoisocaproate $(P_{13C} = 18\%), [^{15}N_3]$ metronidazole $(P_{15N} = 13\%, [c] = 20 \text{ mM})$, and others. While the vast majority of the utility studies have been performed in standard 5 mm NMR tubes, the sample chamber of the device can accommodate a wide range of sample container sizes and geometries of up to 1 L sample volume. The device establishes an integrated, simple, inexpensive, and versatile equipment gateway needed to facilitate parahydrogen-based hyperpolarization experiments ranging from basic science to preclinical applications; indeed, detailed technical drawings and a bill of materials are provided to support the ready translation of this design to other laboratories.

Although MRI has become one of the most useful imaging advances in modern medicine, the very low $(10^{-6}-10^{-5})$ spin polarization P of biomedically relevant spin-1/2 nuclei (1 H, 31 P, 129 Xe, 13 C, and 15 N) makes in vivo imaging of these nuclei challenging at clinically relevant conditions, with the exception of protons of abundant species, e.g., tissue water and fat. However, it is possible to increase P up to the order of unity through the use of hyperpolarization approaches and produce exogenous hyperpolarized (HP) contrast agents for molecular imaging applications. 2,3 In such approaches, nonequilibrium spin polarization is transiently created through the use of NMR

hyperpolarization techniques such as spin exchange optical pumping, 4,5 dissolution dynamic nuclear polarization (d-DNP), 3 parahydrogen-induced polarization (PHIP), 6-9 and other methods. The d-DNP method is the leading

Received: November 19, 2023 Revised: January 15, 2024 Accepted: January 29, 2024 Published: February 15, 2024





hyperpolarization technique for the production of $^{13}C^{11}$ and $^{15}N^{12}$ HP contrast agents. This method relies on the transfer of spin order from unpaired electrons. d-DNP requires complex and expensive (\sim \$1M) equipment and typically long polarization times (\sim 1 h). In contrast, PHIP methods utilize parahydrogen (p-H₂) as a source of spin order and can produce HP contrast agents using inexpensive (\sim \$50–\$100k), fast (\sim 1 min), and relatively simple instrumentation. The resulting p-H₂-hyperpolarized substrates can be employed for in vivo imaging $^{6,22-29}$ and other applications, e.g., reaction monitoring. $^{30-33}$

The two major groups of p-H₂-based hyperpolarization techniques are non-hydrogenative signal amplification by reversible exchange (SABRE)^{34,35} and hydrogenative PHIP. 8,9,36 SABRE technique is based on simultaneous chemical exchange of a $p-H_2$ and to-be-hyperpolarized molecule on a metal center. Both methods rely on $p-H_2$ gas as the source of spin order. 6 Both techniques employ chemical catalysis to bring together a p-H2 molecule and a target nucleus within a few chemical bonds in order to facilitate the polarization transfer from p-H2-derived protons to the target nucleus via spin-spin couplings. A wide range of transfer approaches can be envisioned for p-H2-based polarization (PHIP and SABRE), but they can all be divided into two broad categories. One category of methods employs the application of radiofrequency (RF) pulses to enable polarization transfer,^{37–39} which is typically performed in conventional high-field NMR spectrometers at a magnetic field of a few Tesla, or in a stand-alone hyperpolarizer, typically operating at a field of several mT. A number of PHIP devices employing this method have been reported with detailed descriptions and bills of materials (BOMs). 16-21,40

Another large category of PHIP methods relies on employing static or alternating µT magnetic fields operating to reach level anti-crossing (LAC) regimes, where efficient polarization transfer can occur spontaneously. 41,42 For hydrogenative PHIP, a suitable unsaturated substrate is first hydrogenated with p-H2 in a specific initial magnetic field. This step is typically accomplished at the Earth's field for practical convenience. Next, a magnetic field cycling (MFC)^{43,44} procedure is applied as follows: the field is brought nonadiabatically (i.e., very fast change of magnetic field) to near zero, i.e., sub- μ T. Finally, the magnetic field is increased adiabatically (i.e., gradually changing the magnetic field, allowing the spin system to adapt its configuration⁴⁵) to establish a passage through LACs. This adiabatic field passage results in polarization transfer to the target nucleus (typically ¹³C or ¹⁵N for most biomedical applications) from nascent p- H_2 -derived protons. For the SABRE technique, sub- μT static magnetic fields can be employed to reach LACs between p-H₂derived hydrides and a to-be-HP heteronucleus via spin-spin couplings established on a transiently formed polarization transfer complex (PTC) of a catalyst. This specialized variant of SABRE was called SABRE in SHield Enables Alignment Transfer to Heteronuclei (SABRE-SHEATH). 46,47 It has enabled the SABRE technique to efficiently HP a wide range of biologically relevant molecules with ¹³C and ¹⁵N labels. This category of p-H₂-based hyperpolarization methods requires precise control of the magnetic fields experienced by a sample, which is conveniently achieved using mu-metal magnetic shields and electromagnets. 46,47 Additional requirements include p-H2 gas delivery and temperature control for optimum polarization transfer, with the goal of maximizing polarization gained by the heteronucleus. A number of experimental setups have been developed over the years for this second category of p-H $_2$ hyperpolarization, including the pioneering work from the Malmo group ⁴⁴ and more recent work by TomHon and co-workers. ⁴⁸ However, none of the previous literature reports have provided a complete design of the instrumentation with a BOM that could be readily reproduced by others working in this rapidly expanding field. Moreover, many of these hyperpolarization setups have been designed with the vision of studying novel materials and novel detection approaches in ultralow magnetic fields rather than with the goal of producing a batch of HP contrast agents for biomedical utilization.

Here, we present a complete design of an integrated hyperpolarizer for p-H₂-based hyperpolarization experiments in μT magnetic fields. The device chassis integrates the key components needed to perform hyperpolarization experiments, including a mass flow controller for precise p-H2 flow control, a pressure regulator (for p-H2 gas pressure control), a mu-metal chamber with automated degaussing capability, nonmagnetic temperature regulation, and precise magnetic field control in the μ T magnetic field range (enabled by a solenoid magnet). We also provide examples of hyperpolarization experiments using this hyperpolarizer device for SABRE-SHEATH hyperpolarization of $[^{15}N_3]$ metronidazole (P_{15N} of 13%) and [1- 13 C]pyruvate (P_{13C} of 14%). The utility of the device is also demonstrated for the PHIP-MFC hyperpolarization of ethyl [1-13C]acetate. While the vast majority of the studies have been performed in standard 5 mm NMR tubes (providing convenient means of spectroscopic detection using a wide range of NMR spectrometers), the device chamber can accommodate reaction vessels of over 1 L size, providing a scalable platform for a wide range of studies.

MATERIALS AND METHODS

Design. The mainframe of the device is made from a 30 mm T-slot aluminum extrusion rail (McMaster Carr, P/N 5537T97 and 5537T98, or Misumi, P/N HFS6-3060 and HFS6-3030), chosen due to their nonmagnetic and lightweight nature. This extrusion rail enables the convenient mounting of other auxiliary components. The step-by-step construction of the polarizer skeleton is shown in Figures S4-S12 in the Supporting Information. The front face of the polarizer chassis is divided into five sections for the attachment of 3 mm (or 1/8 in.) thick aluminum plates that are machined for the mounting of device components, Figure 1. Each mounted plate on the front face is dedicated to a specific group of functions of the device: electrical switches, PID temperature control, magnetic field control and degaussing, p-H2 gas flow control (using a mass flow controller), and p-H2 line pressure control (using a pressure regulator). The inside of the chassis is divided into three major compartments, each comprising a temperature control section, the magnetic shields with field control, and the electric wiring unit areas (Figure S13). The technical drawings for all polarizer panels are provided in Figures S21-S29.

To avoid paramagnetic interference of the heating equipment with the mu-metal shields, a nonmagnetic heating/cooling solution was adopted, Figures 1 and 2a. Specifically, a 220 mm-long T-slot aluminum rail (25 mm size) with a 5 mm diameter central hole was employed for heat exchange between the aluminum rail and a 5 mm NMR tube placed inside. The temperature of the aluminum T-slot rail block is maintained by the recirculating-water-filled PVC tubing uniformly coiled

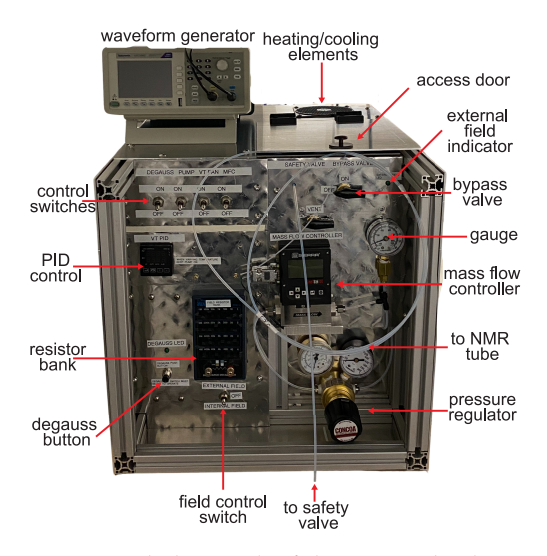


Figure 1. Annotated photograph of the integrated polarizer device outlining the key components. Variable-temperature manifold (heating components) is illustrated in detail in Figure 2 and in the Supporting Information (Figure S14).

around it, Figure 3 and Supporting Information. The ends of the coiled PVC tubing are connected to a heat exchanger, and the water flow inside the tubing is maintained via a miniature water pump (Figure 2b and Supporting Information), with a flow rate of 8 L/min. The heating elements of the heat exchanger are controlled by a PID controller, Figures 1 and 2a,c. Water media inside the PVC tubing was doped with ethylene glycol to prevent foaming and air bubble formation. Our setup can maintain a sample temperature of up to 80 °C. Finally, the thermoelectric cooler (TEC) can be switched on in the case that temperature control below room temperature is needed, Figure 3. In this case, the TEC is constantly turned on to maximum power for chilling, while the PID with heater provides control for temperatures between 8 °C and room temperature.

Parahydrogen gas pressure and flow regulation are integrated by using a brass pressure regulator (Concoa, P/N COA4025301) and mass flow controller (Sierra Instruments, C100L-DD-1-OV1-SV1-PV2-V1-S0-C0), respectively, Figure 3. Parahydrogen enters the device via a through-wall push-to-connect 1/8 in. outer-diameter (OD) Teflon line at the back of the device and flows through the regulator (set to the desired pressure) before it passes through the mass-flow controller and is delivered to the sample for bubbling. A pressure gauge

positioned immediately after the flow controller along the way of the manifold reports on the operating pressure, whereas the mass flow controller display reports on the p-H₂ flow (5-150 standard cubic centimeters per minute, sccm). Since this massflow controller is limited to 130 psi maximum pressure, the total operational pressure range is limited to 100 psi p-H₂ gas overpressure, which is controlled by a safety valve, Figure 3. If a less expensive setup is desired with a higher dynamic p-H₂ gas flow rate and pressure, the mass-flow controller is readily replaced by a brass high-precision threaded flow-adjustment valve (McMaster-Carr, P/N 7832K21), Figure S31. Parahydrogen gas continuously flows through the hyperpolarizer to ensure positive pressure and the removal of any trapped air. When the bypass valve is in the open position, the gas flow is directed via the bypass, and no p-H₂ gas bubbling through the sample occurs. When the bypass valve is closed, the p-H₂ gas is directed to the NMR tube (or other vessel) for bubbling through a liquid sample. Safety and vent valves are connected in series with the bypass valve for pressure relief, Figure 3. Optionally, the gas manifold can be modified by the addition of a saturator vessel (for example, another NMR tube with pure solvent) inline before the NMR tube. The saturator is important for continuous hours-long SABRE-SHEATH experiments as it allows for compensating the gradual solvent evaporation from the sample as a result of gas bubbling.⁴⁹ This saturator system should have its own bypass valve: in this way, one can start and stop p-H₂ gas bubbling through the saturator and the sample independently of each other. One can either use the vent valve for these purposes (i.e., change the gas line connections to the vent valve and use the safety valve for pressure relief) or incorporate an additional (third) valve in the setup.

As reported previously, one challenge frequently encountered in microtesla field experiments is the eventual magnetization of the magnetic shields used, which can lead to substantial undesirable dephasing effects. In this hyperpolarizer, we have integrated a previously developed automated degaussing circuit, Figures 2b and 3. It is based on adiabatic attenuation of input current using thermistors in parallel with a capacitor and the degaussing coil. The circuit allows degaussing the shield to a residual field of less than 20 nT in less than 3 s by pressing the degauss button, Figure 1.

Operation. The device is initiated by a main power switch at the back. Once it is turned on, the PID temperature controller begins temperature regulation, which is usually achieved in 10–15 min. The recirculating pump must be on for temperature-controlled experiments. Next, the field inside

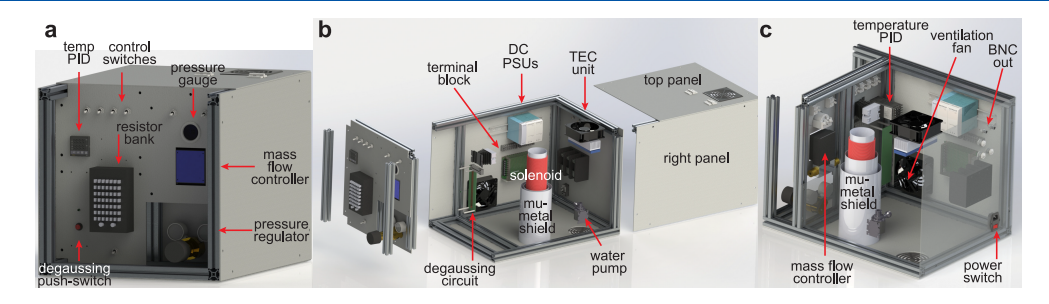


Figure 2. Hyperpolarizer 3D rendering of (a) external view of the device, (b) exploded view of the device, and (c) side view with two panels removed and the back panel transparent. Note that gas tubes and electric wires are not displayed to improve visibility. The minute differences between the 3D renderings presented in this figure versus the annotated photograph shown in Figure 1 are due to the fact that eight copies of the hyperpolarizer have been built and installed so far, with small differences in the component layout in the front and the back panels.

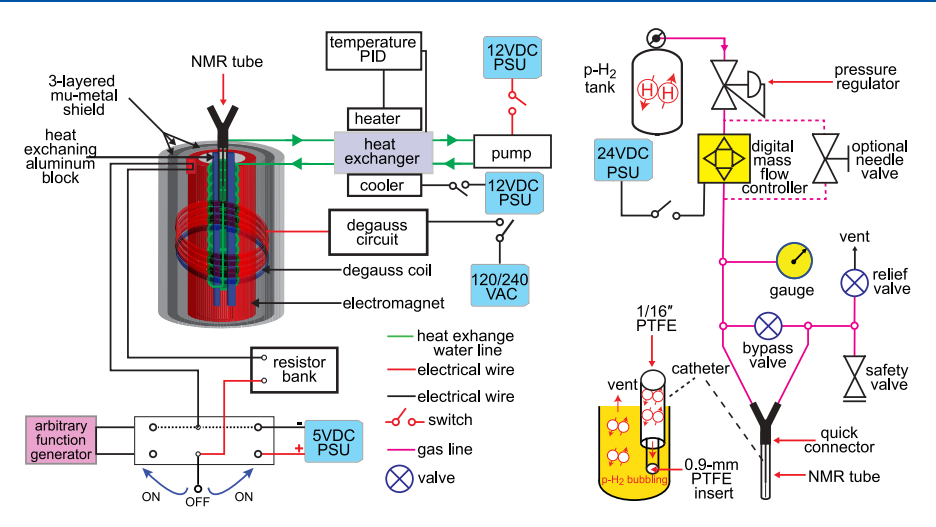


Figure 3. (Left) Schematic of the internal components of the device, showing the electrical connections. (Right) Schematic of the fluid path of the hyperpolarizer, using the example of p-H₂ gas bubbling via a standard 5 mm NMR tube.

the mu-metal shield is measured using a three-axis fluxgate magnetometer (Bartington Instruments, Oxford, UK). If the residual field is not within the desired range, the degaussing button is pressed and released after approximately 2 s (the button is released when the degauss LED light dims off) to demagnetize the shield. It is important to note that the degauss switch is turned on first before pressing the degauss button. This procedure prevents the accidental magnetization of the mu-metal shield due to the unintentional consecutive pressing of the degauss button.

For typical operation, the regulator is set to 130 psi of p-H₂ overpressure, and the p-H₂ input line is pressurized. In our lab, this is established using the p-H₂ distribution system that routes p-H₂ gas via 1/8" OD line to the back of the hyperpolarizer. S2 Alternatively, p-H₂ gas is fed into the device from a p-H₂ tank via 1/8 in. OD PTFE tubing with a push-toconnect through-wall connector on the back panel. Next, the sample in 5 mm NMR tube is connected using a Teflon jacket (made from 0.25"-OD tubing) via a nonmagnetic pushconnect wye adapter (McMaster Carr 5779K262), as shown in Figures 3 and S18.51 Next, the mass-flow controller is turned on using the power switch located on the front panel, and the p-H₂ gas flow rate is set using the control buttons. At this point, the pressure reading on the gauge (Figure 3) starts rising to the set pressure of the safety valve (typically 100 psi). The device is usually purged with incoming p-H₂ for several minutes to remove any trapped air in gas lines. Once the desired p-H₂ pressure is reached and the p-H₂ now exits via the safety valve (with the relief valve closed), the sample is fully pressurized and ready for bubbling. Finally, when the desired temperature is reached and the sample is pressurized, the magnetic field required for the experiment is set using either internal PSU or external AFG, and the hyperpolarization experiment can proceed.

For hyperpolarization experiments (PHIP or SABRE), the liquid sample is bubbled with p-H₂ gas by closing the bypass valve for the desired period of time. When polarization is completed, the valve is switched to the open position to cease the flow of p-H₂ gas (and direct the flow via the bypass). The sample is then transferred to the NMR spectrometer for detection. The p-H₂ bubbling is terminated because there is no more gain in polarization buildup (after the sample is removed from the μ T field) and to minimize susceptibility-induced

magnetic field gradients to prevent otherwise undesirable NMR line broadening.

■ RESULTS AND DISCUSSION

The performance of the hyperpolarizer has been tested in several recently reported PHIP and SABRE-SHEATH hyperpolarization studies. Provided below are illustrative examples of the hyperpolarizer utility for producing $^{13}\mathrm{C}$ and $^{15}\mathrm{N}$ HP solutions of biologically relevant molecules by using SABRE and PHIP hyperpolarization techniques. Approximately 95–98.5% p-H₂ gas was employed for all the experiments described here. 60

SABRE-SHEATH Hyperpolarization of [15N3]-**Metronidazole.** Metronidazole is a FDA-approved antibiotic. Moreover, the detection of HP [15N3]metronidazole in the brain has been recently demonstrated, and the potential utility for hypoxia sensing has been proposed.⁶¹ For [15N₃]metronidazole hyperpolarization, the to-be-hyperpolarized sample employing 2 mM of [IrCl(COD)(IMes)] (IMes = 1,3-bis(2,4,6-trimethylphenyl) imidazole-2-ylidene and COD = 1,5-cyclooctadiene)⁶² polarization transfer precatalyst and 20 mM of [15N₃]metronidazole⁶³ in CD₃OD (0.6 mL aliquot) was placed into a medium-wall 5 mm NMR tube. The sample was bubbled with p-H₂ at room temperature for 1 h at 100 psig using a flow rate of 40 sccm to activate the sample.⁶⁴ After activation was achieved, the sample was bubbled with p-H2 for 1 min (at room temperature, 70 sccm and 100 psi p-H₂ overpressure) to perform SABRE-SHEATH hyperpolarization (Figure 4a) and quickly transferred into a 1.4 T NMR spectrometer (NMR Pro60, Nanalysis) situated right next to the hyperpolarizer for ¹⁵N detection, Figure 4c. A corresponding ¹⁵N spectrum of thermally polarized neat [¹⁵N]pyridine (obtained using 64 scans with a repetition time of 10 min) was employed as a signal reference, Figure 4b. 57,64 Following the detection of the HP signal, the sample was returned back to the hyperpolarizer, where the sample temperature was stabilized for 1 min, and the experiment was repeated (on average, it was possible to repeat SABRE-SHEATH rehyperpolarization of the sample every 4–5 min for 4–5 h). Repeating the experiment at various microtesla fields allows performing a field sweep experiment, Figure 4d, that identifies the optimal hyperpolarization conditions for SABRE-SHEATH, i.e., where the magnetic field matches the LAC⁴² position of the spin system

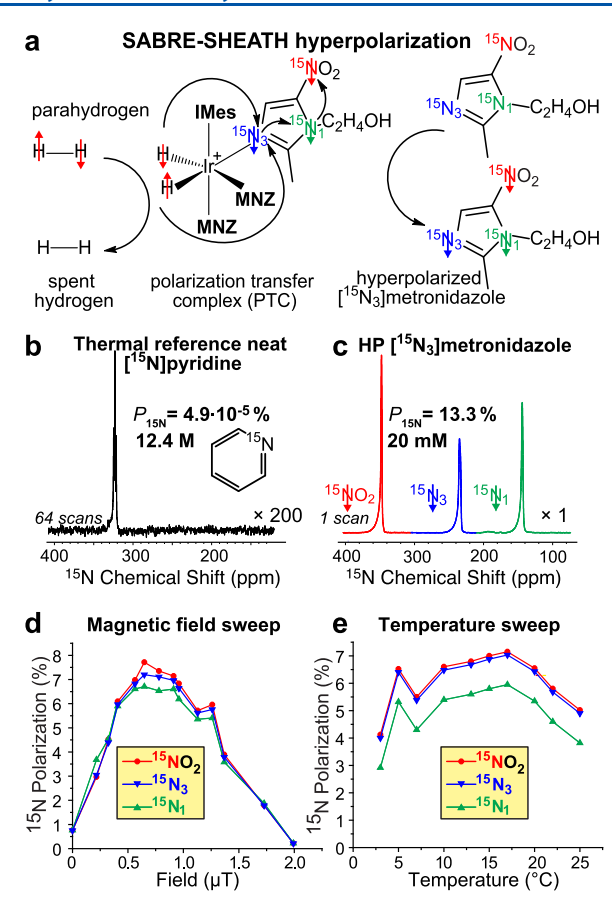


Figure 4. (a) Schematic of spin-relayed SABRE-SHEATH hyper-polarization of $[^{15}N_3]$ metronidazole. (b) ^{15}N spectrum of thermally polarized neat $[^{15}N]$ pyridine (obtained using 64 scans with repetition time of 10 min) used as a signal reference for computing ^{15}N signal enhancement and P_{15N} values. (c) ^{15}N spectrum of HP $[^{15}N_3]$ metronidazole obtained using 1 scan and otherwise the same acquisition parameters. (d) Magnetic field sweep of SABRE-SHEATH process using temperature of ~18 °C. (e) Temperature sweep of SABRE-SHEATH process at a field of 0.6 μT.

participating in the polarization transfer from p-H₂-derived hydrides to the $^{15}\mathrm{N}_3$ nucleus, Figure 4a. 46,47 The spin-relayed polarization transfer mechanism 65 facilitate the polarization transfer from the $^{15}\mathrm{N}_3$ site to the $^{15}\mathrm{N}_1$ site and the $^{15}\mathrm{NO}_2$ site, Figure 4a. 63 Moreover, performing the experiment at the optimal field at various temperatures (i.e., temperature sweep) shown in Figure 4e allows identifying the optimal temperature, corresponding to the optimal rate of chemical exchange of $[^{15}\mathrm{N}_3]$ metronidazole on the PTC, Figure 4a. Using the combination of the optimized temperature (~18 °C) and the field (~0.6 $\mu\mathrm{T}$) in the SABRE-SHEATH experiment allowed the reaching $P_{15\mathrm{N}}$ of 13% on all three $^{15}\mathrm{N}$ sites, Figure 4c. All in all, we conclude that the device provides sufficient reproducibility to enable systematic optimization studies of the temperature and magnetic field, Figure 4.

SABRE-SHEATH Hyperpolarization of [1-¹³C]Pyruvate. HP [1-¹³C]pyruvate is the emerging molecular probe for imaging elevated anaerobic glycolysis, a pathway upregulated in many cancers and other metabolically challenged diseases. Over 50 clinical trials are now pending using HP [1-¹³C]pyruvate as an injectable contrast agent produced via d-DNP technology, according to clinicaltrials.gov. The

SABRE-SHEATH hyperpolarization method presents a cheaper and faster approach to hyperpolarize [1-¹³C]pyruvate, Figure 5a. ^{69,70} We have recently demonstrated that [1-¹³C]-

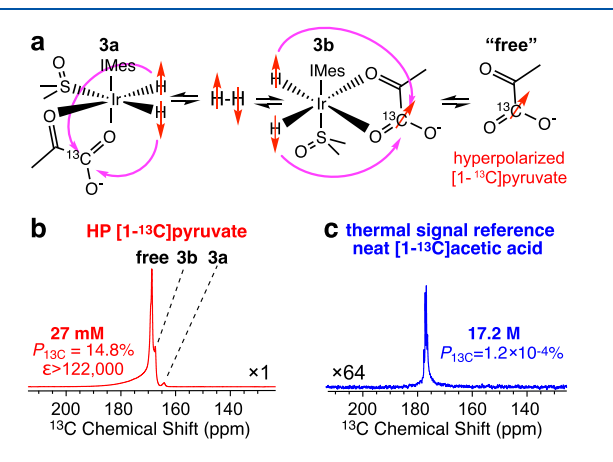


Figure 5. (a) Schematic of simultaneous chemical exchange of p-H₂ and $[1^{-13}C]$ pyruvate on the activated IrIMes PTC complex **3b** to yield "free" HP $[1^{-13}C]$ pyruvate. Complex **3a** undergoes only p-H₂ exchange. (b) ^{13}C NMR spectrum of 27 mM HP sodium $[1^{-13}C]$ pyruvate hyperpolarized via SABRE-SHEATH. (c) Corresponding ^{13}C spectrum of signal reference compound (neat $[1^{-13}C]$ acetic acid). Reprinted with permission from Ref 50 Copyright 2022 ACS.

pyruvate can be hyperpolarized via SABRE-SHEATH up to 14.8% 13 C polarization level 50,53,71 using the following experimental parameters of our hyperpolarizer: 27 mM [1- 13 C] pyruvate, 18 mM DMSO, and 6 mM IMes PTC catalyst in 0.6 mL CD₃OD, activation time of 30 min, polarization time of 1 min with 120 psi p-H₂ overpressure and 120 sccm p-H₂ flow rate, and a pulsed SABRE-SHEATH approach. 50 Other structurally similar α -ketocarboxylates have also been successfully 13 C-hyperpolarized using the hyperpolarizer and similar experimental conditions, including α -ketoglutarate (P_{13C} of up to 17%) 52 and ketoisocaproate (P_{13C} of up to 18%). 56 Moreover, the hyperpolarizer has also been employed for the redissolution (Re-D) SABRE-SHEATH method that yields a biocompatible aqueous solution of HP [1- 13 C] pyruvate with a P_{13C} of 9%.

PHIP-MFC Hyperpolarization of Ethyl [1-13C]Acetate. Due to the ease with which it is taken up by the brain cells, ¹³C-labeled acetate has been used for brain metabolic tracing in rats and humans by magnetic resonance spectroscopy. 72,73 HP [1-13C]acetate (produced by d-DNP) has also been used for the investigation of other metabolic transformations in the TCA cycle.⁷⁴ Hyperpolarizing acetate and pyruvate via side arm hydrogenation (SAH) PHIP have been demonstrated by Reineri and co-workers. In the PHIP-SAH method, a precursor molecule with an unsaturated side arm is hydrogenated with p-H2, and then the singlet order obtained on the product protons is converted into magnetization on ¹³C using MFC. 44,75-77 Following the ¹³C hyperpolarization of the unsaturated precursor, e.g., using vinyl arm hydrogenation shown in Figure 6a, the arm can be cleaved by hydrolysis for the production of HP [1-13C]acetate or [1-13C]pyruvate.⁷⁵ The hyperpolarizer was employed for the production of HP ethyl [1-13C]acetate using the PHIP-SAH method, Figure 6a, via the MFC procedure, Figure 6b. Briefly, 0.6 mL of 0.5-1 M of vinyl [1-13C] acetate in acetone with 10 mM rhodium-based

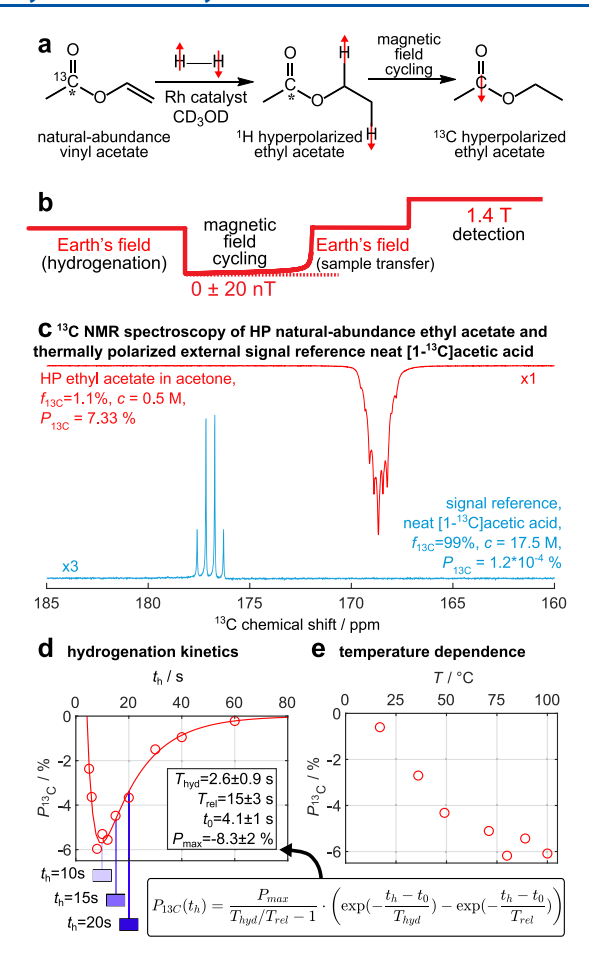


Figure 6. (a) Hyperpolarization reaction of vinyl $[1^{-13}C]$ acetate with p-H₂ to form 1H HP ethyl $[1^{-13}C]$ acetate, which is field-cycled to yield ^{13}C HP ethyl $[1^{-13}C]$ acetate. (b) The overall scheme of MFC. (c) ^{13}C spectrum of HP ethyl $[1^{-13}C]$ acetate using manual field cycling (0.5 M, red trace) and corresponding ^{13}C spectrum of thermally polarized signal reference of neat $[1^{-13}C]$ acetic acid (17.5 M, blue trace). All spectra are acquired using a 9° flip angle of the RF excitation pulse. (d) p-H₂-based hyperpolarization kinetics of 0.5 M vinyl acetate (VA) conversion to HP ethyl acetate at 80 °C with 10 mM catalyst concentration. (e) Temperature dependence of P_{13C} at 1 M VA and 10 mM catalyst concentrations and hydrogenation time ($T_{\rm hyd}$) of 10 s. Reproduced with permission from Ref 58 Copyright 2023 Wiley.

catalyst (1,4-bis(diphenylphosphino)butane(1,5cyclooctadiene)rhodium(I) tetrafluoroborate ([Rh(dppb)-(COD)]BF₄), Strem 45-0190, CAS 79255-71-3) was measured into a regular-wall 5 mm NMR tube and heated for 15 s at 80 °C in the Earth's field. 58,59 The sample was then shuttled into the hyperpolarizer's mu-metal shield and then slowly pulled out in 5 s before being transferred for ¹³C detection with a 1.4 T benchtop NMR spectrometer, Figure 6c. 58,59 Comparison of HP signal intensity with the signal intensity obtained from thermally polarized reference (neat [1-13C]acetic acid, Figure 6c) allowed determining P_{13C} of up to 7.33%, Figure 6c.⁵⁸ The robust operation of the device enabled optimization of hyperpolarization kinetics (Figure 6d) and reaction temperature (Figure 6e) with the goal of maximizing the degree of ¹³C polarization. ^{58,59} Achieving the relatively high level of ¹³C polarization at high substrate concentrations was useful to demonstrate the feasibility of creating ¹³C radio amplification by stimulated emission of radiation. ^{58,59} While the manual

MFC approach was used for hyperpolarization of ethyl [1-¹³C]acetate, Figure 6, the AFG can be programmed for automated operation (see Supporting Information for details). Indeed, the automated procedure has been implemented recently using the polarizer prototype, demonstrating the feasibility of performing PHIP-SAH hyperpolarization studies using natural ¹³C abundance and a benchtop spectrometer. ⁷⁸ We envision that other biomolecules ⁷⁹ can also be amenable to PHIP-SAH hyperpolarization using our device.

Outlook. The key limitation of the reported hyperpolarizer device is the lack of automation and the focus on hyperpolarization of small-size samples intended for detection in 5 mm NMR tubes. At the same time, the simplicity and low cost of the device clearly highlight the benefits of the reported design. We envision that the relatively large chamber of the solenoid magnet can, in principle, enable the use of a substantially larger reaction chamber, and sample sizes over 1 L can, in principle, be accommodated. At the same time, the small scale of polarization in 5 mm NMR tubes reported here is large enough to produce a dose of the ¹³C contrast agent for its utility in mice and rats. ^{24,25,56} We also envision that other biologically relevant molecules can be hyperpolarized using the reported hyperpolarization via SABRE-SHEATH approach and pulsed-SABRE-SHEATH approaches because all enabling functionalities are indeed available in the reported hyperpolarizer. 35,80 Moreover, while the feasibility demonstrations of hyperpolarization processes have been performed using a large (ca. 10 L size) aluminum cylinder⁶⁰ containing compressed p-H₂ gas, the reported device can potentially utilize p-H₂ gas packed in cheap and disposable pressurized aluminum cans, an approach that may further reduce the cost and complexity of hyperpolarizer operation, especially in the proximity of MRI

It should also be noted that a number of approaches have been recently demonstrated to enable the production of biocompatible aqueous solutions of HP [1-13C]pyruvate using the gas manifold and other components employed in the reported hyperpolarizer design. ^{24,25,55,82} Two of these recent advances reported on HP [1-13C]pyruvate production via SABRE-SHEATH in 5 mm NMR tubes and its utilization for metabolic imaging of HP [1-13C]pyruvate in mice and rats.²⁴ Therefore, the reported hyperpolarizer design can be readily employed for preclinical studies using the emerging new protocols for the production of biocompatible formulations of HP [1-¹³C]pyruvate already. We envision that these methods for the production of biocompatible solutions of HP media can be expanded to other biologically relevant HP molecular probes for their in vivo utilization in the near future. However, it should be noted that the reported hyperpolarizer design is not approved for clinical utilization.

CONCLUSIONS

We have presented a hyperpolarizer for performing p-H₂-based hyperpolarization experiments in microtesla magnetic fields. The device has been designed with an emphasis on simplicity and low cost (less than \$7000 in components, ca. 2021, when it was developed and first constructed). The device can be conveniently sited near a NMR spectrometer^{50,52–56} for high-resolution characterization and optimization of the hyperpolarization processes or in the proximity of a MRI scanner⁵⁶ to perform rapid hyperpolarization of substrates for utilization in small animals. Moreover, the hyperpolarizer can easily be relocated between different sites due to its compact footprint

and quick start time. The utility of the hyperpolarizer has been demonstrated for the hyperpolarization of a wide range of biologically relevant molecules, including most notably $[1^{-13}C]$ pyruvate ($P_{13C}=14\%$). Future improvements of the reported hyperpolarizer are envisioned in the areas of automation, process optimization (i.e., the development of high-pressure and high-flow reaction vessels for p-H₂ bubbling), demonstration of larger production volumes and quantities of HP biomolecules (all the way to clinical scale), and implementation of new approaches and chemistries to mitigate the toxicity of p-H₂-HP solutions that frequently contain catalysts and organic solvents. All in all, the reported open-source design bodes well for the future development and widespread use of p-H₂-HP injectable contrast agents.

ASSOCIATED CONTENT

5 Supporting Information

The Supporting Information is available free of charge at https://pubs.acs.org/doi/10.1021/acs.analchem.3c05233.

Additional experimental details, materials and methods including photographs, schematics, computer codes and examples of their output, itemized schematics, and BOM of the hyperpolarizer, assembly instructions, and exploded view diagrams (PDF)

AUTHOR INFORMATION

Corresponding Authors

Shiraz Nantogma — Department of Chemistry, Integrative Biosciences (Ibio), Wayne State University, Karmanos Cancer Institute (KCI), Detroit, Michigan 48202, United States; Email: nantogmashiraz@wayne.edu

Eduard Y. Chekmenev — Department of Chemistry, Integrative Biosciences (Ibio), Wayne State University, Karmanos Cancer Institute (KCI), Detroit, Michigan 48202, United States; Russian Academy of Sciences, Moscow 119991, Russia; orcid.org/0000-0002-8745-8801; Email: chekmenevlab@gmail.com

Authors

Md Raduanul H. Chowdhury – Department of Chemistry, Integrative Biosciences (Ibio), Wayne State University, Karmanos Cancer Institute (KCI), Detroit, Michigan 48202, United States

Mohammad S. H. Kabir — Department of Chemistry, Integrative Biosciences (Ibio), Wayne State University, Karmanos Cancer Institute (KCI), Detroit, Michigan 48202, United States

Isaiah Adelabu — Department of Chemistry, Integrative Biosciences (Ibio), Wayne State University, Karmanos Cancer Institute (KCI), Detroit, Michigan 48202, United States; orcid.org/0000-0002-9475-0851

Sameer M. Joshi – Department of Chemistry, Integrative Biosciences (Ibio), Wayne State University, Karmanos Cancer Institute (KCI), Detroit, Michigan 48202, United States

Anna Samoilenko — Department of Chemistry, Integrative Biosciences (Ibio), Wayne State University, Karmanos Cancer Institute (KCI), Detroit, Michigan 48202, United States

Henri de Maissin – German Cancer Consortium (DKTK), Partner Site Freiburg, German Cancer Research Center (DKFZ), Heidelberg 69120, Germany; Division of Medical Physics, Department of Diagnostic and Interventional Radiology, University Medical Center Freiburg, Faculty of Medicine, University of Freiburg, Freiburg 79106, Germany

Andreas B. Schmidt – Department of Chemistry, Integrative Biosciences (Ibio), Wayne State University, Karmanos Cancer Institute (KCI), Detroit, Michigan 48202, United States; German Cancer Consortium (DKTK), Partner Site Freiburg, German Cancer Research Center (DKFZ), Heidelberg 69120, Germany; Division of Medical Physics, Department of Diagnostic and Interventional Radiology, University Medical Center Freiburg, Faculty of Medicine, University of Freiburg, Freiburg 79106, Germany; orcid.org/0000-0001-8944-7463

Panayiotis Nikolaou − XeUS Technologies LTD, Nicosia 2312, Cyprus; ⊙ orcid.org/0000-0002-3802-0803

Yuri A. Chekmenev – XeUS Technologies LTD, Nicosia 2312, Cyprus

Oleg G. Salnikov – International Tomography Center SB RAS, Novosibirsk 630090, Russia; orcid.org/0000-0003-2266-7335

Nikita V. Chukanov – International Tomography Center SB RAS, Novosibirsk 630090, Russia

Igor V. Koptyug – International Tomography Center SB RAS, Novosibirsk 630090, Russia; orcid.org/0000-0003-3480-7649

Boyd M. Goodson — School of Chemical & Biomolecular Sciences and Materials Technology Center, Southern Illinois University, Carbondale, Illinois 62901, United States;

orcid.org/0000-0001-6079-5077

Complete contact information is available at: https://pubs.acs.org/10.1021/acs.analchem.3c05233

Notes

The authors declare the following competing financial interest(s): P.N., B.M.G., and E.Y.C. declare a stake of ownership in XeUS Technologies, LTD. E.Y.C. holds stock of Vizma Life Sciences (VLS) and serves on the scientific advisory board (SAB) of VLS.

ACKNOWLEDGMENTS

This work was supported by DOD CDMRP under BRP W81XWH-12-1-0159/BC112431, NSF CHE-1905341, CHE-1904780, and NIBIB R21 EB033872. B.M.G. acknowledges a Cottrell SEED grant from the Research Corporation for Science Advancement. O.G.S. and N.V.C. thank the Russian Science Foundation (grant 21-73-10105) for the support of polarizer optimization and tests in SABRE-SHEATH studies at ITC SB RAS. A.B.S. acknowledges support by the German Cancer Consortium (DKTK) and the German Research Foundation (DFG #SCHM 3694/1-1, #SCHM 3694/2-1, #SFB1479). A.B.S. and E.Y.C. thank Wayne State University for a Postdoctoral Fellow award.

REFERENCES

- (1) Eills, J.; Budker, D.; Cavagnero, S.; Chekmenev, E. Y.; Elliott, S. J.; Jannin, S.; Lesage, A.; Matysik, J.; Meersmann, T.; Prisner, T.; et al. *Chem. Rev.* **2023**, *123* (4), 1417–1551.
- (2) Barskiy, D. A.; Coffey, A. M.; Nikolaou, P.; Mikhaylov, D. M.; Goodson, B. M.; Branca, R. T.; Lu, G. J.; Shapiro, M. G.; Telkki, V.-V.; Zhivonitko, V. V.; et al. *Chem.—Eur. J.* **2017**, 23 (4), 725–751.
- (3) Ardenkjaer-Larsen, J. H.; Fridlund, B.; Gram, A.; Hansson, G.; Hansson, L.; Lerche, M. H.; Servin, R.; Thaning, M.; Golman, K. *Proc. Natl. Acad. Sci. U.S.A.* **2003**, *100* (18), 10158–10163.

- (4) Walker, T. G.; Happer, W. Rev. Mod. Phys. 1997, 69 (2), 629–642.
- (5) Khan, A. S.; Harvey, R. L.; Birchall, J. R.; Irwin, R. K.; Nikolaou, P.; Schrank, G.; Emami, K.; Dummer, A.; Barlow, M. J.; Goodson, B. M.; et al. *Angew. Chem., Int. Ed.* **2021**, *60* (41), 22126–22147.
- (6) Hövener, J.; Pravdivtsev, A. N.; Kidd, B.; Bowers, C. R.; Glöggler, S.; Kovtunov, K. V.; Plaumann, M.; Katz-Brull, R.; Buckenmaier, K.; Jerschow, A.; et al. *Angew. Chem., Int. Ed.* **2018**, 57 (35), 11140–11162.
- (7) Green, R. A.; Adams, R. W.; Duckett, S. B.; Mewis, R. E.; Williamson, D. C.; Green, G. G. R. Prog. Nucl. Magn. Reson. Spectrosc. 2012, 67, 1–48.
- (8) Bowers, C. R.; Weitekamp, D. P. Phys. Rev. Lett. 1986, 57 (21), 2645-2648.
- (9) Eisenschmid, T. C.; Kirss, R. U.; Deutsch, P. P.; Hommeltoft, S. I.; Eisenberg, R.; Bargon, J.; Lawler, R. G.; Balch, A. L. *J. Am. Chem. Soc.* 1987, 109 (26), 8089–8091.
- (10) Hirsch, M. L.; Kalechofsky, N.; Belzer, A.; Rosay, M.; Kempf, J. G. J. Am. Chem. Soc. **2015**, 137 (26), 8428–8434.
- (11) Brindle, K. M. J. Am. Chem. Soc. 2015, 137 (20), 6418-6427.
- (12) Park, H.; Wang, Q. Chem. Sci. 2022, 13 (25), 7378-7391.
- (13) Kurhanewicz, J.; Vigneron, D. B.; Brindle, K.; Chekmenev, E. Y.; Comment, A.; Cunningham, C. H.; DeBerardinis, R. J.; Green, G. G.; Leach, M. O.; Rajan, S. S.; et al. *Neoplasia* **2011**, *13* (2), 81–97.
- (14) Ardenkjaer-Larsen, J. H. J. Magn. Reson. 2016, 264, 3-12.
- (15) Schmidt, A. B.; Berner, S.; Schimpf, W.; Müller, C.; Lickert, T.; Schwaderlapp, N.; Knecht, S.; Skinner, J. G.; Dost, A.; Rovedo, P.; et al. *Nat. Commun.* **2017**, *8*, 14535.
- (16) Schmidt, A. B.; Bowers, C. R.; Buckenmaier, K.; Chekmenev, E. Y.; de Maissin, H.; Eills, J.; Ellermann, F.; Glöggler, S.; Gordon, J. W.; Knecht, S.; et al. *Anal. Chem.* **2022**, *94* (1), 479–502.
- (17) Hoevener, J.-B.; Chekmenev, E. Y.; Harris, K. C.; Perman, W. H.; Robertson, L. W.; Ross, B. D.; Bhattacharya, P. Magn. Reson. Mater. Phys. 2009, 22 (2), 111–121.
- (18) Hoevener, J.-B.; Chekmenev, E. Y.; Harris, K. C.; Perman, W. H.; Tran, T. T.; Ross, B. D.; Bhattacharya, P. *Magn. Reson. Mater. Phys.* **2009**, 22 (2), 123–134.
- (19) Coffey, A. M.; Shchepin, R. V.; Truong, M. L.; Wilkens, K.; Pham, W.; Chekmenev, E. Y. *Anal. Chem.* **2016**, 88 (16), 8279–8288.
- (20) Coffey, A. M.; Shchepin, R. V.; Feng, B.; Colon, R. D.; Wilkens, K.; Waddell, K. W.; Chekmenev, E. Y. J. Magn. Reson. 2017, 284, 115–124.
- (21) Kadlecek, S.; Vahdat, V.; Nakayama, T.; Ng, D.; Emami, K.; Rizi, R. NMR Biomed. **2011**, 24 (8), 933–942.
- (22) Bhattacharya, P.; Chekmenev, E. Y.; Reynolds, W. F.; Wagner, S.; Zacharias, N.; Chan, H. R.; Bünger, R.; Ross, B. D. *NMR Biomed.* **2011**, 24 (8), 1023–1028.
- (23) Hune, T.; Mamone, S.; Schroeder, H.; Jagtap, A. P.; Sternkopf, S.; Stevanato, G.; Korchak, S.; Fokken, C.; Müller, C. A.; Schmidt, A. B.; et al. *ChemPhysChem* **2023**, 24 (2), No. e202200615.
- (24) MacCulloch, K.; Browning, A.; Guarin Bedoya, D. O.; McBride, S. J.; Abdulmojeed, M. B.; Dedesma, C.; Goodson, B. M.; Rosen, M. S.; Chekmenev, E. Y.; Yen, Y.-F.; et al. *J. Magn. Reson. Open* **2023**, 16–17, 100129.
- (25) de Maissin, H.; Groß, P. R.; Mohiuddin, O.; Weigt, M.; Nagel, L.; Herzog, M.; Wang, Z.; Willing, R.; Reichardt, W.; Pichotka, M.; et al. *Angew. Chem., Int. Ed.* **2023**, *62*, No. e202306654.
- (26) Gierse, M.; Nagel, L.; Keim, M.; Lucas, S.; Speidel, T.; Lobmeyer, T.; Winter, G.; Josten, F.; Karaali, S.; Fellermann, M.; et al. *J. Am. Chem. Soc.* **2023**, *145* (10), 5960–5969.
- (27) Golman, K.; Axelsson, O.; Johannesson, H.; Mansson, S.; Olofsson, C.; Petersson, J. S. Magn. Reson. Med. 2001, 46 (1), 1-5.
- (28) Stewart, N. J.; Nakano, H.; Sugai, S.; Tomohiro, M.; Kase, Y.; Uchio, Y.; Yamaguchi, T.; Matsuo, Y.; Naganuma, T.; Takeda, N.; et al. *ChemPhysChem* **2021**, 22 (10), 915–923.
- (29) Bhattacharya, P.; Chekmenev, E. Y.; Perman, W. H.; Harris, K. C.; Lin, A. P.; Norton, V. A.; Tan, C. T.; Ross, B. D.; Weitekamp, D. P. J. Magn. Reson. **2007**, 186, 150–155.

- (30) Semenova, O.; Richardson, P. M.; Parrott, A. J.; Nordon, A.; Halse, M. E.; Duckett, S. B. *Anal. Chem.* **2019**, *91* (10), 6695–6701.
- (31) Barskiy, D. A.; Kovtunov, K. V.; Primo, A.; Corma, A.; Kaptein, R.; Koptyug, I. V. *ChemCatChem* **2012**, *4* (12), 2031–2035.
- (32) Bouchard, L. S.; Burt, S. R.; Anwar, M. S.; Kovtunov, K. V.; Koptyug, I. V.; Pines, A. Science 2008, 319 (5862), 442-445.
- (33) Mandal, R.; Pham, P.; Hilty, C. Chem. Sci. 2021, 12 (39), 12950–12958.
- (34) Adams, R. W.; Aguilar, J. A.; Atkinson, K. D.; Cowley, M. J.; Elliott, P. I. P.; Duckett, S. B.; Green, G. G. R.; Khazal, I. G.; López-Serrano, J.; Williamson, D. C. Science 2009, 323 (5922), 1708–1711.
- (35) Salnikov, O. G.; Burueva, D. B.; Skovpin, I. V.; Koptyug, I. V. *Mendeleev Commun.* **2023**, 33 (5), 583–596.
- (36) Bowers, C. R.; Weitekamp, D. P. J. Am. Chem. Soc. 1987, 109 (18), 5541-5542.
- (37) Lindale, J. R.; Eriksson, S. L.; Warren, W. S. Phys. Chem. Chem. Phys. **2022**, 24 (12), 7214–7223.
- (38) Bär, S.; Lange, T.; Leibfritz, D.; Hennig, J.; Elverfeldt, D. v.; Hövener, J. B. J. Magn. Reson. 2012, 225, 25–35.
- (39) Pravdivtsev, A. N.; Hövener, J.; Schmidt, A. B. ChemPhysChem **2022**, 23 (3), No. e202100721.
- (40) Waddell, K. W.; Coffey, A. M.; Chekmenev, E. Y. J. Am. Chem. Soc. **2011**, 133 (1), 97–101.
- (41) Pravdivtsev, A. N.; Yurkovskaya, A. V.; Lukzen, N. N.; Vieth, H.-M.; Ivanov, K. L. Phys. Chem. Chem. Phys. 2014, 16 (35), 18707—18719
- (42) Ivanov, K. L.; Pravdivtsev, A. N.; Yurkovskaya, A. V.; Vieth, H.-M.; Kaptein, R. Prog. Nucl. Magn. Reson. Spectrosc. 2014, 81, 1-36.
- (43) Goldman, M.; Johannesson, H.; Axelsson, O.; Karlsson, M. Magn. Reson. Imaging 2005, 23 (2), 153-157.
- (44) Johannesson, H.; Axelsson, O.; Karlsson, M. C. R. Phys. **2004**, *5* (3), 315–324.
- (45) Born, M.; Fock, V. Z. Phys. 1928, 51 (3-4), 165-180.
- (46) Theis, T.; Truong, M. L.; Coffey, A. M.; Shchepin, R. V.; Waddell, K. W.; Shi, F.; Goodson, B. M.; Warren, W. S.; Chekmenev, E. Y. J. Am. Chem. Soc. 2015, 137 (4), 1404–1407.
- (47) Truong, M. L.; Theis, T.; Coffey, A. M.; Shchepin, R. V.; Waddell, K. W.; Shi, F.; Goodson, B. M.; Warren, W. S.; Chekmenev, E. Y. J. Phys. Chem. C 2015, 119 (16), 8786-8797.
- (48) TomHon, P. M.; Han, S.; Lehmkuhl, S.; Appelt, S.; Chekmenev, E. Y.; Abolhasani, M.; Theis, T. *ChemPhysChem* **2021**, 22 (24), 2526–2534.
- (49) Blanchard, J. W.; Ripka, B.; Suslick, B. A.; Gelevski, D.; Wu, T.; Münnemann, K.; Barskiy, D. A.; Budker, D. *Magn. Reson. Chem.* **2021**, 59 (12), 1208–1215.
- (50) Nantogma, S.; Eriksson, S. L.; Adelabu, I.; Mandzhieva, I.; Browning, A.; TomHon, P.; Warren, W. S.; Theis, T.; Goodson, B. M.; Chekmenev, E. Y. J. Phys. Chem. A 2022, 126 (48), 9114–9123.
- (51) Joalland, B.; Nantogma, S.; Chowdhury, M. R. H.; Nikolaou, P.; Chekmenev, E. Y. *Magn. Reson. Chem.* **2021**, 59 (12), 1180–1186.
- (52) Adelabu, I.; Ettedgui, J.; Joshi, S. M.; Nantogma, S.; Chowdhury, M. R. H.; McBride, S.; Theis, T.; Sabbasani, V. R.; Chandrasekhar, M.; Sail, D.; et al. *Anal. Chem.* **2022**, *94* (39), 13422–13431.
- (53) Adelabu, I.; TomHon, P.; Kabir, M. S. H.; Nantogma, S.; Abdulmojeed, M.; Mandzhieva, I.; Ettedgui, J.; Swenson, R. E.; Krishna, M. C.; Theis, T.; et al. *ChemPhysChem* **2022**, 23 (2), No. e202100839.
- (54) Mandzhieva, I.; Adelabu, I.; Chekmenev, E. Y.; Theis, T. ACS Sens. 2022, 7 (12), 3773-3781.
- (55) Schmidt, A. B.; de Maissin, H.; Adelabu, I.; Nantogma, S.; Ettedgui, J.; TomHon, P.; Goodson, B. M.; Theis, T.; Chekmenev, E. Y. ACS Sens. 2022, 7 (11), 3430–3439.
- (56) Adelabu, I.; Chowdhury, M. R. H.; Nantogma, S.; Oladun, C.; Ahmed, F.; Stilgenbauer, L.; Sadagurski, M.; Theis, T.; Goodson, B. M.; Chekmenev, E. Y. *Metabolites* **2023**, *13* (2), 200.
- (57) Kabir, M. S. H.; Joshi, S. M.; Samoilenko, A.; Adelabu, I.; Nantogma, S.; Gelovani, J. G.; Goodson, B. M.; Chekmenev, E. Y. J. Phys. Chem. A 2023, 127 (23), 5018–5029.

- (58) Nelson, C.; Schmidt, A. B.; Adelabu, I.; Nantogma, S.; Kiselev, V. G.; Abdurraheem, A.; de Maissin, H.; Lehmkuhl, S.; Appelt, S.; Theis, T.; et al. *Angew. Chem., Int. Ed.* **2023**, *135* (5), No. e202215678.
- (59) Schmidt, A. B.; Adelabu, I.; Nelson, C.; Nantogma, S.; Kiselev, V. G.; Zaitsev, M.; Abdurraheem, A.; de Maissin, H.; Rosen, M. S.; Lehmkuhl, S.; et al. *J. Am. Chem. Soc.* **2023**, *145* (20), 11121–11129. (60) Nantogma, S.; Joalland, B.; Wilkens, K.; Chekmenev, E. Y. *Anal. Chem.* **2021**, *93* (7), 3594–3601.
- (61) Guarin, D. O.; Joshi, S. M.; Samoilenko, A.; Kabir, M. S. H.; Hardy, E. E.; Takahashi, A. M.; Ardenkjaer-Larsen, J. H.; Chekmenev, E. Y.; Yen, Y.-F. Angew. Chem., Int. Ed. 2023, 62 (31), No. e202219181.
- (62) Cowley, M. J.; Adams, R. W.; Atkinson, K. D.; Cockett, M. C. R.; Duckett, S. B.; Green, G. G. R.; Lohman, J. A. B.; Kerssebaum, R.; Kilgour, D.; Mewis, R. E. *J. Am. Chem. Soc.* **2011**, *133* (16), 6134–6137.
- (63) Shchepin, R. V.; Birchall, J. R.; Chukanov, N. V.; Kovtunov, K. V.; Koptyug, I. V.; Theis, T.; Warren, W. S.; Gelovani, J. G.; Goodson, B. M.; Shokouhi, S.; et al. *Chem.—Eur. J.* **2019**, 25, 8829–8836.
- (64) Birchall, J. R.; Kabir, M. S. H.; Salnikov, O. G.; Chukanov, N. V.; Svyatova, A.; Kovtunov, K. V.; Koptyug, I. V.; Gelovani, J. G.; Goodson, B. M.; Pham, W.; et al. *Chem. Commun.* **2020**, *56* (64), 9098–9101.
- (65) Shchepin, R. V.; Jaigirdar, L.; Theis, T.; Warren, W. S.; Goodson, B. M.; Chekmenev, E. Y. J. Phys. Chem. C 2017, 121 (51), 28425–28434.
- (66) Kiryutin, A. S.; Yurkovskaya, A. V.; Ivanov, K. L. ChemPhysChem 2021, 22 (14), 1470-1477.
- (67) Kurhanewicz, J.; Vigneron, D. B.; Ardenkjaer-Larsen, J. H.; Bankson, J. A.; Brindle, K.; Cunningham, C. H.; Gallagher, F. A.; Keshari, K. R.; Kjaer, A.; Laustsen, C.; et al. *Neoplasia* **2019**, *21* (1), 1–16.
- (68) Wang, Z. J.; Ohliger, M. A.; Larson, P. E. Z.; Gordon, J. W.; Bok, R. A.; Slater, J.; Villanueva-Meyer, J. E.; Hess, C. P.; Kurhanewicz, J.; Vigneron, D. B. *Radiology* **2019**, 291 (2), 273–284.
- (69) Iali, W.; Roy, S. S.; Tickner, B. J.; Ahwal, F.; Kennerley, A. J.; Duckett, S. B. *Angew. Chem., Int. Ed.* **2019**, 58 (30), 10271–10275.
- (70) TomHon, P.; Abdulmojeed, M.; Adelabu, I.; Nantogma, S.; Kabir, M. S. H.; Lehmkuhl, S.; Chekmenev, E. Y.; Theis, T. *J. Am. Chem. Soc.* **2022**, *144* (1), 282–287.
- (71) Chapman, B.; Joalland, B.; Meersman, C.; Ettedgui, J.; Swenson, R. E.; Krishna, M. C.; Nikolaou, P.; Kovtunov, K. V.; Salnikov, O. G.; Koptyug, I. V.; et al. *Anal. Chem.* **2021**, 93 (24), 8476–8483.
- (72) Bluml, S.; Moreno-Torres, A.; Shic, F.; Nguy, C. H.; Ross, B. D. *NMR Biomed.* **2002**, *15* (1), 1–5.
- (73) Cerdan, S.; Künnecke, B.; Seelig, J. J. Biol. Chem. 1990, 265 (22), 12916–12926.
- (74) Mishkovsky, M.; Comment, A.; Gruetter, R. J. Cereb. Blood Flow Metab. 2012, 32 (12), 2108-2113.
- (75) Reineri, F.; Boi, T.; Aime, S. Nat. Commun. 2015, 6, 5858.
- (76) Rodin, B. A.; Eills, J.; Picazo-Frutos, R.; Sheberstov, K. F.; Budker, D.; Ivanov, K. L. *Phys. Chem. Chem. Phys.* **2021**, 23 (12), 7125–7134.
- (77) Cavallari, E.; Carrera, C.; Boi, T.; Aime, S.; Reineri, F. J. Phys. Chem. B **2015**, 119 (31), 10035–10041.
- (78) Joalland, B.; Chekmenev, E. Y. J. Phys. Chem. Lett. 2022, 13, 1925–1930.
- (79) Reineri, F.; Cavallari, E.; Carrera, C.; Aime, S. Magn. Reson. Mater. Phys. **2021**, 34, 25–47.
- (80) Colell, J. F. P.; Logan, A. W. J.; Zhou, Z.; Shchepin, R. V.; Barskiy, D. A.; Ortiz, G. X.; Wang, Q.; Malcolmson, S. J.; Chekmenev, E. Y.; Warren, W. S.; et al. *J. Phys. Chem. C* **2017**, *121* (12), 6626–6634.
- (81) Ariyasingha, N. M.; Samoilenko, A.; Birchall, J. R.; Chowdhury, M. R. H.; Salnikov, O. G.; Kovtunova, L. M.; Bukhtiyarov, V. I.; Zhu, D. C.; Qian, C.; Bradley, M.; et al. *ACS Sens.* **2023**, *8* (10), 3845–3854.

(82) Ettedgui, J.; Blackman, B.; Raju, N.; Kotler, S. A.; Chekmenev, E. Y.; Goodson, B. M.; Merkle, H.; Woodroofe, C. C.; LeClair, C. A.; Krishna, M. C.; et al. *J. Am. Chem. Soc.* **2024**, *146* (1), 946–953.